Beam collimation for CSNS/RCS

WEI Tao(魏涛)[1] WU Qing-Biao(吴青彪)[1] LI Wen-Qian(李文茜)[2]

[1] Institute of High Energy Physics, CAS, Beijing 100049, China
[2] Department of Physics Engineering, Tsinghua University, Beijing 100084, China

Abstract The current design of the CSNS/RCS beam collimation system consists of a two-stage betatron collimation and a single momentum collimator. This paper summarizes various aspects of collimator design, including collimation principle and layout, material choice and collimator mechanical structure, etc. At last, radiation and thermal analysis are carried out to illustrate the feasibility of the current beam collimation scheme.

Key words collimation, beam loss, collimator

PACS 29.27.Eg, 33.80.-b

1 Introduction

In a high intensity proton ring, collimations are needed in order to maintain reasonable levels of residual activation and allow hands-on maintenance. Here, we put the emphasis on low energy, high intensity accelerators such as the Chinese Spallation Neutron Source (CSNS) rapid cycling synchrotron (RCS) to be constructed in Dongguan, Guangdong Province, China.

The condition of hands-on maintenance requires that the average residual radiation in the tunnel does not exceed 1 mSv/h (measured at 30 cm away from the device surface, 4 hours after machine shutdown). Experimental and numerical studies indicate 1–2 watt [1] of beam power per tunnel meter as an upper limit for uncontrolled beam loss.

To achieve hands-on maintenance and high machine availability, collimators are placed at strategic positions around the ring to remove particles outside the beam core and to localize beam losses in special zones. These locations will then become the only "hot spots" of the machine in which remote handling is required. Even if the beam is lost in the collimators, we consider it a controlled beam loss.

In this paper, we describe the collimation system design for both betatron collimation and momentum collimation in the ring. In Section 2 we summarize the two-stage betatron collimation system [2] and the detailed structure of collimators, including the primary collimator (scraper) and the secondary collimator (absorber). The description of the momentum collimator is given in Section 3. In Section 4 we present the initial results on the residual dose and thermal analysis.

2 Betatron collimation

The advantage of the two-stage collimation system compared with the single collimator was acknowledged. As far as the CSNS/RCS two-stage betatron collimation system is concerned, thin metallic scrapers are used as a primary collimator to interact with the halo particles and increase their impact parameters on the secondary collimators. To do so the collimation efficiency can be significantly improved.

The present betatron collimation system is arranged in a dedicated straight section as shown in Fig. 1. To adapt to the existing lattice we put the primary collimator in front of the secondary drift (9.3 m), and the following four secondary collimators which occupy suitable phase advances from the primary one.

Because of the space charge effect, the emittance of the beam increases slowly. These slow growing halo particles may hit the primary collimator at very small impact parameters. As a result, protons leave the primary collimator with the amplitudes larger than or equal to the primary collimator's acceptance ε_1 and actually with any angular coordinates. These scraped

Received 30 April 2009

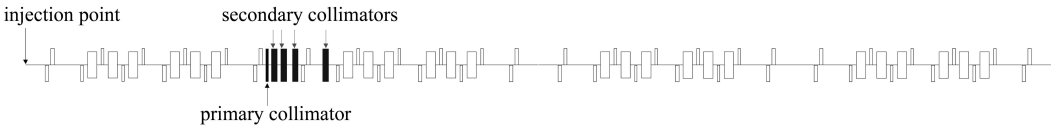

Fig. 1. Location of the betatron collimators in CSNS/RCS.

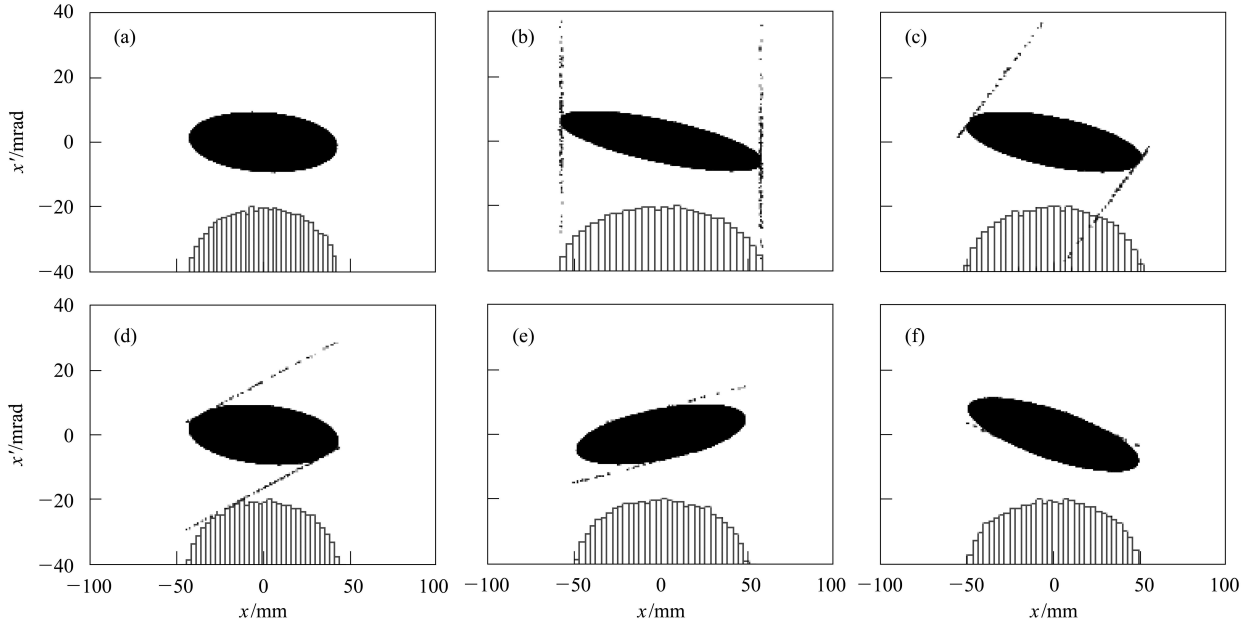

Fig. 2. Horizontal phase space at the injection point (a), at the primary collimator (b), and at the following four secondary collimators (c)–(f).

particles have to be absorbed by the secondary collimators downstream from the primary collimator at an acceptance of $\varepsilon_2 > \varepsilon_1$ [3]. How the betatron collimation system functions is shown in Fig. 2.

The secondary collimators need to be placed at phase advances which are optimal to intercept most of particles out-scattered from the primary collimator during the first turn. The optimum phase advances are $\mu_{\rm opt} = \arccos\sqrt{\varepsilon_1/\varepsilon_2} \approx 22°$ and its complement of 158° [4]. For the limitation of the current lattice, the betatron phases of absorbers with respect to scraper are chosen as 10°/10°, 32°/28°, 79°/59°, 123°/151°.

2.1 Primary collimator

The primary collimator is a kind of jaw-type one, the chief components are thin scrapers which have adjustable distance to the beam center. Once the primary collimator is in place inside the machine it becomes the main aperture restriction. For easier operation, a special design consisting of a movable inner surface for the primary collimator was proposed. Fig. 3 shows the structural figure of the primary collimator.

The reactions which occur in the primary collimator mainly are multiple scattering and ionization energy loss. They were well formulated by Molière's theory and Bethe-Block equation [5], respectively. Suitable material and length of scrapers are very important to the design of the primary collimator. On one hand, we expect the deposited energy in the scrapers is as less as possible. On the other hand, the scraper has to kick the halo particles enough to drive them into the secondary collimators with large impact parameters. That is to say, the ideal scraper should produce both a small energy loss and large average multiple Coulomb scattering angle. Table 1 shows the average scattering angle for different materials whose thicknesses have been adjusted to have an average momentum loss of 1% for 100 MeV protons.

The scattering angle of carbon and aluminum is too small, and the iron and copper do not have any advantage in the view of scattering angle and melting point. Tungsten is difficult to be processed, and platinum is too expensive. Overall, tantalum is the most suitable material for scraper. Finally we choose 0.14 mm long tantalum as the scraper of the primary collimator.

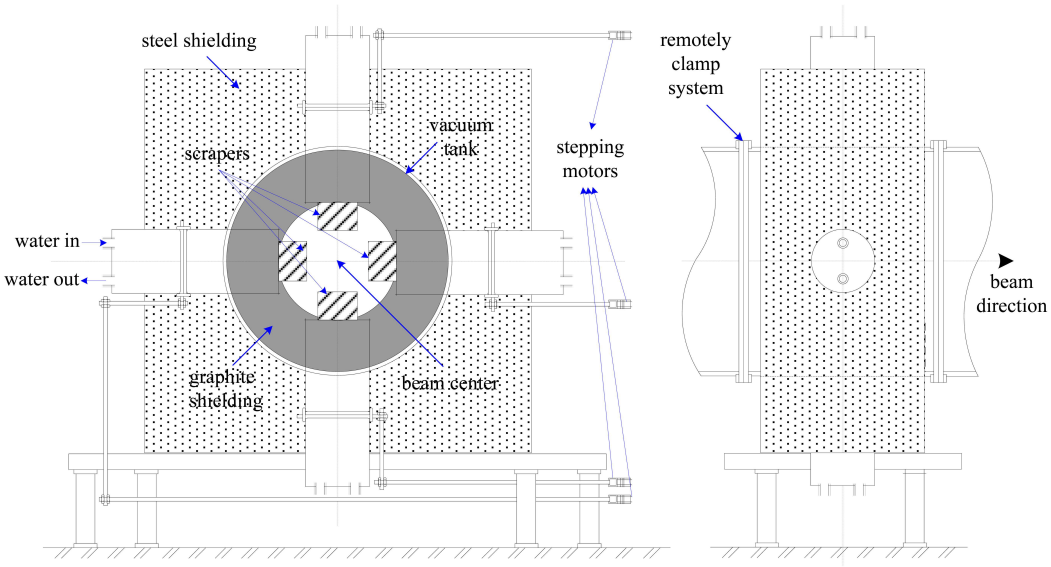

Fig. 3. The schematic view of the primary collimator.

Table 1. Comparison of different scraper materials.

material	density/(g/cm^3)	radlength/cm	melting point/℃	length/mm	mCs angle/mrad	λ/(W·m^{-1}·K^{-1})
C	2.27	18.8	3850	1.25	4.71	∼500
Al	2.7	8.9	660	1.2	6.93	210
Fe	7.87	1.76	1535	0.47	10.1	76.2
Cu	8.92	1.43	1083	0.43	10.7	385
Ta	16.6	0.411	2996	0.3	17.5	54.4
W	19.3	0.35	3410	0.26	17.7	163.3
Pt	21.5	0.305	1772	0.24	18.1	69.1

λ: coefficient of thermal conductivity.

2.2 Secondary collimator

The secondary collimators are self-shielding structures capable of absorbing the scattering halo particles and containing the shower of secondary particles.

Graphite is the favoured material for absorbers, principally because of the low prompt secondary production and quickly decaying activation products. Also, its low atomic mass increases the volume over which energy is deposited, and reduces heating and thermal stress problems.

In the first step of design, the absorber must stop the scattering protons. The lost particles' kinetic energy is lower than 200 MeV in the first stage of CSNS and lower than 400 MeV in the second stage. So the absorber should stop protons with 400 MeV kinetic energy at least and absorb most of the energy of the probably beam loss in 1.6 GeV.

The main mechanism of high energy particles losing their energy in a target is ionization. We can use Bethe-Bloch formula to estimate the Continuous-Slowing-Down-Approximation (CSDA) range of protons in absorber. The CSDA range of 400 MeV proton in graphite is about 50 cm.

What is shown in Fig. 4 is the schematic view of the secondary collimator. The main material is graphite and water-cooled device because the graphite is a good neutron moderator. The secondary neutrons will be slowed down through inelastic and elastic scattering with graphite block. The reaction is written as

$$\begin{aligned} &{}^{12}_{6}\mathrm{C}+{}^{1}_{0}\mathrm{n}\rightarrow{}^{12}_{6}\mathrm{C}+\gamma+{}^{1}_{0}\mathrm{n}, \quad \text{(inelastic scattering)} \\ &(E_\gamma \geqslant 4.43\ \text{MeV}), \\ &{}^{12}_{6}\mathrm{C}+{}^{1}_{0}\mathrm{n}\rightarrow{}^{12}_{6}\mathrm{C}+{}^{1}_{0}\mathrm{n}. \quad \text{(elastic scattering)}. \end{aligned} \tag{1}$$

Here we use light water as the refrigerant, and we should consider the reaction between neutron and ^{1}H nuclei

$$ {}^{1}_{1}\mathrm{H}+{}^{1}_{0}\mathrm{n}\rightarrow{}^{2}_{1}\mathrm{H}+\gamma. \quad (E_\gamma \geqslant 2.2\ \text{MeV}). \tag{2}$$

We must consider how to prevent these high energy gamma rays. In fact, we will install radiation protection material in the outer of collimators to absorb the high energy rays.

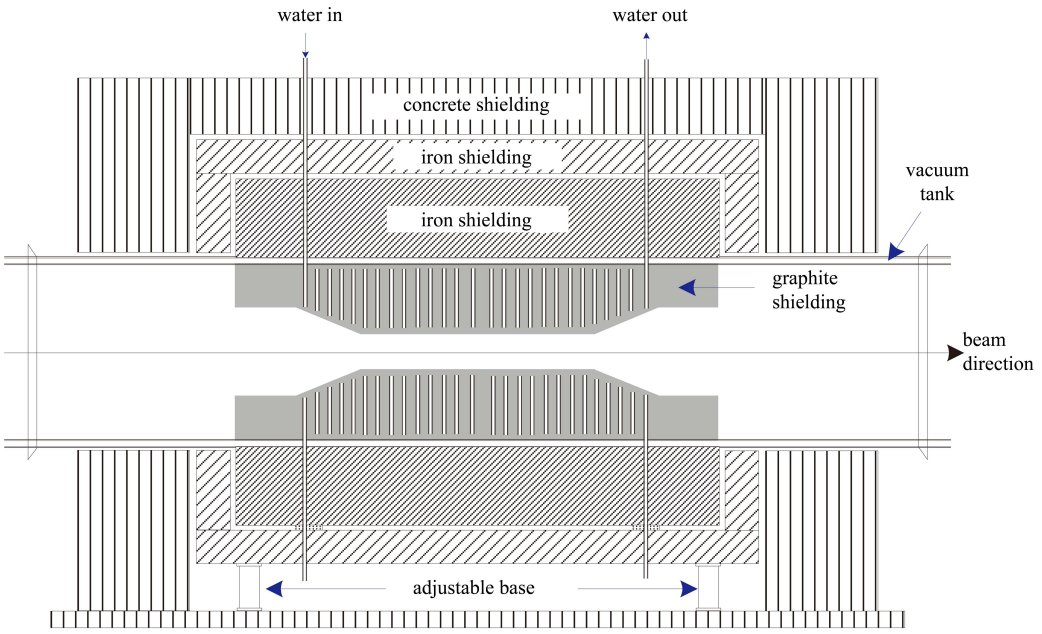

Fig. 4. The schematic view of the secondary collimator.

3 Momentum collimation

The careful designing of CSNS, in particular chopping in the linac, means general momentum losses should be very small. However, it is likely that there will be some longitudinal loss, including (1) loss due to RF trapping inefficient; (2) loss due to error conditions; and (3) loss due to leakage from the betatron collimation. Therefore, the momentum collimation is included.

The momentum collimation limits are chosen such that the beam must exceed both the betatron collimation limit (360 πmm·mrad), and the momentum limit (1%). Placing collimation behind the normal betatron limit, for the beam within the momentum acceptance, allows more particles to be removed by the larger, more fully shielding betatron system. The high dispersion region in the current lattice provides a good condition for momentum collimation. A double jawed collimator is placed as close as possible to the dispersion peak and act as the momentum collimator.

The efficiency of the momentum collimator is highly dependent on the growth rate of the loss. The typical halo growth rate is about 10–100 μm/turn in most accelerators. For longitudinal losses in the CSNS ring, the momentum growth rate of $\sim 1\times10^{-4}$/turn is expected. Combining with the dispersion more than 5 m, the growth rate of particles interacting with the momentum collimator is about 500 μm/turn. A single collimator is tolerable for such a fast growth rate.

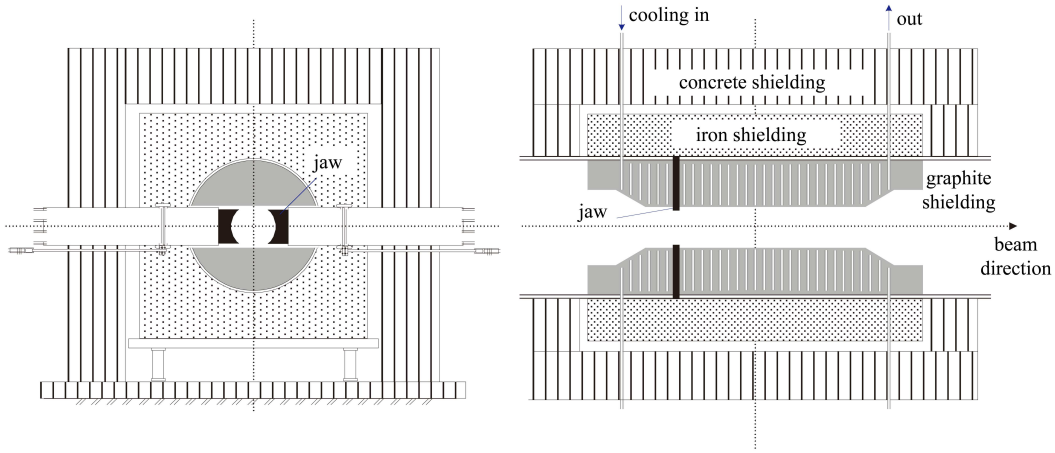

Fig. 5. The schematic view of the momentum collimator.

The schematic figure of momentum collimator is shown in Fig. 5. The length of the momentum collimator is about 3.5 m and the copper jaws are 2 cm long. To prevent the copper jaws from arriving their melting point and decreasing the lifetime of the momentum collimator, we should use water-cooling in the jaws design. According to the simulation results, the momentum collimation efficiency is about 90.6% which meets the needs.

4 Radiation and thermal analysis

Most lost particles concentrate on the secondary collimators (∼93.8%), especially on the first absorber (∼45.3%). The radiation problem of the absorber is most serious, so we perform the radiation analysis of the absorber.

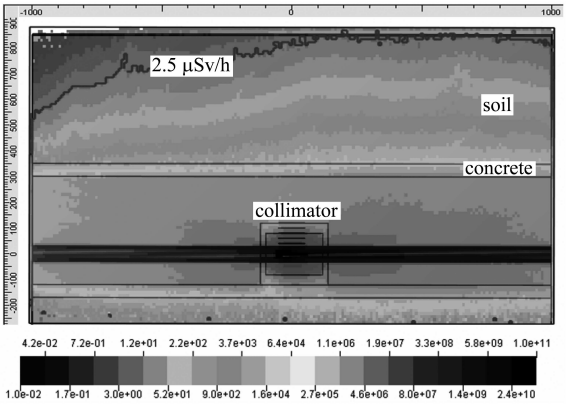

Fig. 6. Total prompt dose rate distribution of the secondary collimator (unit: μSv/h).

Both prompt radiation and induced radiation should follow the requirements:

(1) Prompt radiation: prompt dose rate in non-controlled areas on accessible outside surfaces of the shield is no more than 2.5 μSv/h in normal operation.

(2) Induced radiation: residual dose rate is no more than 1 mSv/h at 30 cm from the component surface, after 100 days irradiation and 4 hours later from shutdown.

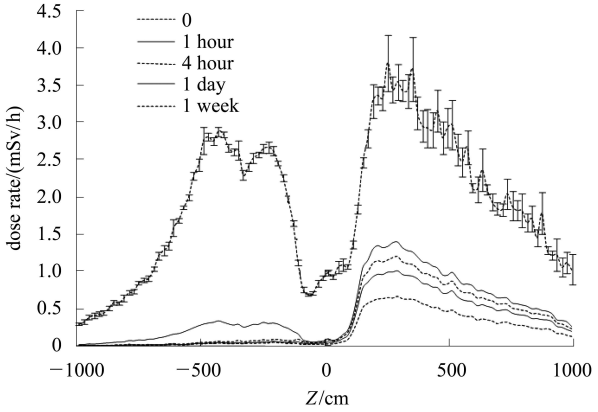

Fig. 7. Residual dose rate at 30 cm from the secondary collimator surface after 100days irradiation and at different cooling time after shut down.

To optimize shielding conditions of the secondary collimator, Monte Carlo code FLUKA was used. Fig. 6 shows a geometric model of RCS tunnel and prompt dose rate distribution due to both 2 kW beam

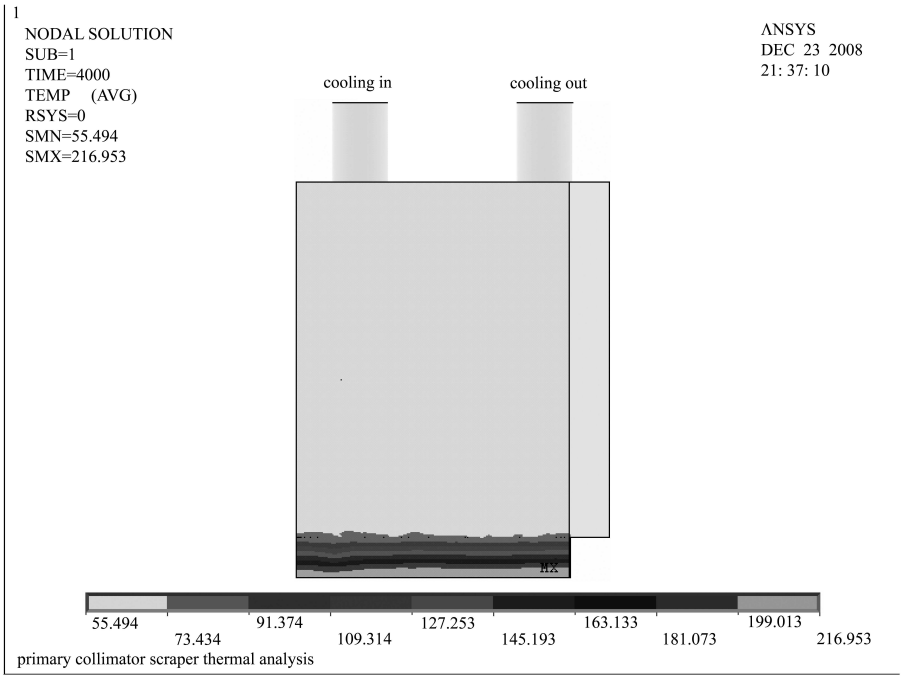

Fig. 8. Thermal analysis of the primary collimator.

loss at the secondary collimator and 1 W/m beam loss along the beam duct. The top tunnel shield includes 50 cm concrete shield and 5 m soil shield. The collimator, centered in the middle of the 20 m long tunnel, has three shielding layers outside: a 30 cm thick graphite shielding, a 49 cm thick iron shield and a 40 cm thick concrete shield. It can be seen from the figure, at ground surface, the prompt dose rate is just below the prompt radiation criteria.

Figure 7 shows the corresponding induced radiation dose rate at 30 cm after 100 days irradiation at 4 hrs after shutdown. We can see it also meets the 1mSv/h residual dose rate criteria.

The heating of the primary collimator is most severe. On the one hand, interaction between halo particles and scraper leads to a large amount of thermal deposition; on the other hand, the scraper is too thin to direct the cooling water.

What is shown in Fig. 8 is the thermal analysis of the primary collimator. The scraper adhered with a copper sheet in which the cooling water cycles. The maximum temperature of the scraper is about 200 degrees which is far below the copper's melting point.

The radiation and thermal analysis shows that the current collimators' structure is feasible. Further study on optimization will continue.

References

1 Catalan-Lasheras N et al. In: Proceedings of the 7th ICFA Mini-Workshop on High Intensity High Brightness Hadron Beams, Lake Como, Wisconsin, 1999. Edited by Mokhov N, Chou W. Fermi National Laboratory, Batavia, Illinois. 1999

2 WEI Tao, QIN Q. NIMA, 2006, **566**: 212–217

3 Jeanneret J B, Renkler T T. Part. Accel., 1995, **50**: 287–311

4 Jeanneret J B. Phys. Rev. ST Accel. Beams, 1998, **1**: 081001

5 XIE Yi-Gang et al. Particle Detectors and Data Acquisition. Beijing: Science Press, 2003. 5–12 (in Chinese)